Impact of *Streptococcus pneumoniae* biosynthesis gene mutations on epithelial microinvasion and cellular responses

Caroline M. Weight[1*], Gabriele Pollara[1], Modupeh Betts[1], Roberta Ragazzini[2], Michael Connor[3], Elisa Ramos-Sevillano[4], Jesús Reiné[5], Matthew Whelan[1], José Afonso Guerra-Assunção[1], Paola Bonfanti[1,2], Clare Jolly[1], Mahdad Noursadeghi[1], Daniela M. Ferreira[5], Jeremy S. Brown[4], Robert S. Heyderman[1]

[1]Research Department of Infection, Division of Infection and Immunity, UCL London, UK

[2]Francis Crick Institute, London, UK

[3]Chromatin and Infection, Institut Pasteur, France

[4]Department of Respiratory Medicine, UCL, London, UK

[5]Oxford Vaccine Group, University of Oxford, Oxford and Clinical Sciences, Liverpool School of Tropical Medicine, Liverpool, UK

*Current address Biomedical and Life Sciences, Faculty of Health and Medicine, Lancaster University, UK

Corresponding Author: Dr Caroline M. Weight

Email: c.weight@lancaster.ac.uk

ABSTRACT

The influence of *Streptococcus pneumoniae* metabolism on nasal epithelial interactions is under-explored. We have assessed *S. pneumoniae* mutations affecting glutamate 5 kinase (*proABC*) and formate tetrahydrofolate reductase (*fhs*). A Pia iron transporter (*piaA*) mutation was added to ensure attenuation in Experimental Human Pneumococcal Challenge (EHPC).

Epithelial microinvasion by Δ*proABC/piaA* and Δ*fhs/piaA* strains was enhanced compared to wild-type (WT) in EHPC and Detroit 562 cell infection. In primary epithelium, acetylated tubulin and β catenin expression was increased following Δ*proABC* exposure and uteroglobin expression was increased with Δ*fhs* exposure. In Detroit 562 cells, WT and Δ*proABC* infection induced an inflammatory epithelial transcriptomic response. The Δ*fhs/piaA* strain induced primarily cellular stress/ repair gene responses. Differential caspase 3/7/8 activity appeared linked to pneumococcal pneumolysin activity and hydrogen peroxide secretion.

Our findings highlight the broad-ranging effects of single gene mutations in pneumococcal metabolism which underlies the complexity of the differences between seemingly closely related pneumococci.

GRAPHICAL ABSTRACT

Bacterial transcriptomics revealed profound effects of biosynthesis gene mutations on bacterial gene expression under serum stress, with upregulation of bacterial virulence factors such as pneumolysin and hydrogen peroxide regulator genes (e.g. *spxB)*. Epithelial microinvasion by the isogenic mutants was increased compared to wild type strain, but bacterial load was not sufficient to account for the differences observed in epithelial gene expression. Deletion of the *fhs* gene induced a more intrinsic cellular stress and repair response, compared to the wild-type strain or deletion of the *proABC* operons which induced a more typical pro-inflammatory response. Differential effects were also seen

in cellular re-modelling and caspase activity. We postulate that this link between bacterial metabolism and virulence under conditions of stress will ultimately influence the outcome of colonisation in terms of transmission potential, transition to disease and generation of protective immunity.

INTRODUCTION

Adaptation to the host environment is crucial for successful colonisation of the upper respiratory tract by a range of human pathogens, including bacteria, viruses and fungi. This includes the ability to withstand different ambient temperatures, overcome physical barriers such as mucus, evade epithelial cellular soluble mediators such as antimicrobial peptides, compete with neighbouring polymicrobial communities and compensate for nutrient restriction. *Streptococcus pneumoniae* (the pneumococcus) is a common bacterial commensal of the human upper respiratory tract (URT), but life-threatening pneumococcal disease can occur following translocation of the bacteria into the lungs, the blood or the brain[1]. Indeed, among children under 5yrs, *S. pneumoniae* is the leading cause of pneumonia deaths globally[2].

Using Experimental Human Pneumococcal Challenge (EHPC) of healthy volunteers and well-characterised epithelial cell models, we have previously shown that colonisation is characterised by epithelial surface microcolony formation and microinvasion (evidence of epithelial invasion and transmigration without disease)[3]. We showed that a *S. pneumoniae* serotype 4 strain (TIGR4) invades Detroit 562 nasopharyngeal epithelial cells more readily than serotype 6B and 23F strains, resulting in a marked pro-inflammatory epithelial transcriptomic and cytokine profile[3]. Therefore, an intracellular lifestyle during carriage may allow the pneumococcus to avoid an adverse URT and induce an epithelial-innate immune response. This led us to propose that epithelial microinvasion and the subsequent inflammatory response may contribute to both bacterial clearance and the promotion of pneumococcal transmission[3].

S. pneumoniae is highly variable with more than 100 serotypes as determined by polysaccharide capsule, and more than 600 underlying global pneumococcal sequence clusters[4]. Pneumococcal virulence, transmissibility and the potential to cause invasive disease are widely recognised as strain dependent, influenced by the polysaccharide capsule, and a wide range of subcapsular and cytoplasmic proteins and other factors[5]. Bacterial cellular metabolism including carbohydrate, nucleotide and amino acid biosynthesis have also been shown to play an important role in the outcome of host-pneumococcal interactions[6-9].

Here we reveal that despite attenuation of disease following disruption of *S. pneumoniae* biosynthetic genes, microinvasion was preserved as a feature of pneumococcal colonisation in both *in vivo* and *in vitro* models. Crucially, we show that the differential downstream effects of microinvasion, including the innate epithelial immune/ inflammatory response and cellular remodelling, are not simply related to bacterial load, but are determined by bacterial metabolism and virulence, coupled to differing bacterial responses to stress. Our findings emphasise the complexity of the epithelial response to bacterial microinvasion during nasopharyngeal colonisation.

RESULTS

To explore the potential mechanisms that link bacterial metabolism to epithelial microinvasion and inflammation during pneumococcal colonisation, and to avoid the confounders of different capsular or genetic backgrounds, we have used isogenic mutants of *S. pneumoniae* serotype 6B which have deletions of key biosynthesis genes; a γ-glutamyl phosphate reductase (*proA*), a γ-glutamyl kinase (*proB*) and a pyrroline-5-carboxylate reductase s (*proC*), collectively referred to as *proABC*; a folate tetrahydrofolate reductase (*fhs*); and then together with a deletion of pneumococcal iron acquisition A (*piaA*)[10]. This double deletion ensures reversion does not occur during host experimental challenge, in the EHPC model[11]. In a murine model, we have previously shown that compared to the *S. pneumoniae* serotype 6B wild-type (WT, BHN418), the Δ*proABC/piaA* and Δ*fhs/piaA* mutants

effectively colonise the nasopharynx but are attenuated in their ability to cause disease[12]. In the EHPC model, both mutants retained the ability to colonise and induced IgG antibody production in colonised individuals[11]. We therefore focussed on the interactions of the Δ*proABC/piaA* and Δ*fhs/piaA* mutant strains with epithelial cells to retain comparability with the human infection experiments.

Deletions of *proABC* and *fhs* genes cause different broad-ranging effects on *S. pneumoniae* metabolism under stress conditions.

We have previously determined the wider impact of the *proABC* and *fhs* mutations on the pneumococcal transcriptome in response to human serum, representing the physiological stress conditions found during human infection[13]. After growth to mid-log phase in THY enriched media and then transferred to human serum for 60 minutes, we found marked transcriptional differences between the WT and both mutants in response to serum stress, with over a three-fold increase in the number of upregulated genes by the mutant strains compared to WT[13]. Genes differentially upregulated by the mutant strains during serum stress included well-characterised pneumococcal virulence factors such as *ply*, *nanA*, *psaA,* those regulating oxidative stress such as *lctO*, and genes involved in purine and carbohydrate metabolism (Supplementary Table 1).

Enrichment analysis of pathways of upregulated genes revealed that phosphotransferase systems, amino nucleotide sugar, fructose and mannose and metabolic pathways were the most significantly enriched pathways in the Δ*proABC* mutant under serum stress (Table 1). There was no disruption in purine pathways or galactose metabolism in this mutant strain. Enrichment pathway analysis for the Δ*fhs* mutant under stress conditions revealed gene upregulation in competence, purine, pyruvate, metabolic pathways, amino nucleotide sugar pathways and secondary metabolites (Table 1). Together these data suggests that deletion of *proABC* and *fhs*, has widespread but different

effects on *S. pneumoniae* metabolism which we postulate may have important effects on the host innate immune response during niche adaptation during colonisation.

S. pneumoniae 6B with _proABC_ or _fhs_ mutations experimentally colonise humans with enhanced microinvasion.

We then tested whether the effects of these gene deletions on metabolism and subsequent growth in sera also affected epithelial cell internalisation (microinvasion) in humans. Nasal curette samples from healthy volunteers inoculated with the 6B WT or double mutant strains *(*Δ*proABC/piaA* or Δ*fhs/piaA*)[14] were collected to investigate the extent of epithelial association and microinvasion, (Figure 1A). A positive carrier was defined as colonisation at any time point (day 2 or day 6 post-inoculation) within the study by microbiology culture (colony forming units, CFU counts) following a nasal wash[3]. Mucosal cells collected by curettage were visualised by confocal microscopy for analysis of direct interactions of the pneumococcal strains with the epithelium (Figure 1B). Colonisation was achieved with all strains as analysed by microbiology and microscopy (Supplemental Information Table 2). Unexpectedly, the day 6 post challenge samples revealed a trend for greater microinvasion by both the Δ*proABC/piaA* or Δ*fhs/piaA* strains compared to WT (Figure 1C), with a higher microinvasive index (percentage of internalised bacteria / associated bacteria) as shown in Figure 1D.

Epithelial microinvasion is not dependent on bacterial load.

We have previously demonstrated that the pattern of microinvasion and the subsequent epithelial innate immune response to *S. pneumoniae* 6B seen *in vitro* with Detroit 562 cells, a human nasopharyngeal carcinoma cell line, is similar to that seen in the EPHC model *in vivo*[3]. Therefore, we used our Detroit 562 cell model to confirm the differences between the Δ*proABC/piaA* or Δ*fhs/piaA* strains compared to WT in microinvasion. We found that, as with the EHPC data, although all strains still interacted with the epithelium forming surface colonies (Figure 2A), the isogenic mutant strains associated less compared to 6B WT (Figure 2B), significantly so for the Δ*fhs/piaA* and Δ*fhs* strains. For all strains, microinvasion was observed with comparable absolute numbers of

internalised bacteria (Figure 2C), therefore resulting in a significantly elevated micro-invasive index for the Δ*proABC/piaA* or Δ*fhs/piaA* strains compared to WT (Figure 2D). Importantly, for the single 6B mutant Δp*iaA* strain, epithelial association and microinvasion were not affected. There were no significant differences in WT and mutant strain intracellular viability, with all strains showing an approximately 50% reduction in intracellular CFU over 3 hours (Figure 1E). However, despite the increased microinvasive index compared to WT, the single Δ*proABC* or Δ*fhs* and the double Δ*proABC/piaA* or Δ*fhs/piaA* strains were impaired in their ability to transmigrate across the epithelium (Figure 1F). This finding is in keeping with previous evidence of disease attenuation in murine models[12]. Similar trends for these strain interactions with epithelial cells were also observed after one hour infection, suggesting bacterial replication does not play an important role in explaining the differences observed between strains (Supplemental Information Figure 1).

Consistent with our previous findings for serotype 6B with Detroit 562 cells and Calu3 cells (a bronchial epithelial cell line)[3], epithelial barrier function was not compromised after three hours of infection; indeed, there was a tightening of the barrier evidenced by reduced FITC dextran diffusion after pneumococcal exposure (Figure 2G). We found no evidence to suggest an impact on of pneumococcal infection on Junctional Adhesion Molecule A (JAM-A), Zonula-Occludens 1 (ZO-1), Claudin 1 or Claudin 4 expression (Supplemental Figure 2). However, we did observe significant increases in β catenin expression following incubation with Δ*proABC/piaA* or Δ*fhs/piaA* strains, compared to non-infected or WT infected cells (Figure 2H, 2I). As measured by secretion of lactate dehydrogenase (LDH), following infection with the *S. pneumoniae* strains, compared to non-infected cells, we detected only a modest (but statistically significant for Δ*proABC/piaA* infection) increase in cell death after six hours (Figure 2J).

S. pneumoniae colonisation and microinvasion of primary human airway epithelium leads to cellular remodelling.

To further explore the impact of microinvasion on epithelial biology in a more complex environment, we cultured *S. pneumoniae* serotype 6B and the isogenic biosynthesis mutants with primary human bronchial epithelial airway (NHBE-A) cells in air-liquid interface. Again, we found that all strains associated with epithelial cells (Figure 3A, top) and were also detected inside epithelial cells, enclosed within vacuoles as detected by TEM (Figure 3A, bottom). To evaluate the differential effects on barrier function, we assessed junctional protein expression and barrier integrity. As previously described[3], 6B WT and mutant strains co-localised with Junctional Adhesion Molecule A (JAM-A, Supplemental Information Figure 3A, arrow), with no change in overall JAM-A expression. However, we did observe an increase in Zonula Occludens 1 (ZO-1) intensity at the junctional membrane for cells infected with the 6B WT strain (Supplementary Figure 3B), and a significant increase in the intensity of β catenin staining for cells infected with Δ*proABC/piaA or* Δ*fhs/piaA* strain (Figure 3B, 3C). Interestingly, β catenin staining in cells exposed to, but not associated with Δ*proABC/piaA* strain were also significantly higher, suggesting paracrine signalling from the epithelium. There were no adverse effects on barrier integrity, as measured by transepithelial electrical resistance (Figure 3D), or cell death as measured by the release of lactate dehydrogenase (LDH, Figure 3E) over the infection period.

When cultured in an air-liquid interface, NHBE cells differentiate into typical respiratory epithelium cell types: Goblet, Clara, Basal and Ciliated cells (Figure 4A). Although we found no evidence to suggest the pneumococcus preferentially colonised particular cell-types, pneumococci were observed to be caught-up within cilia (acetylated tubulin positive cells, Figure 4B and Supplemental Information Figure 4) and co-localised with mucus (mucin5ac positive, Figure 4C, arrows). Strikingly, while the cellular composition of the epithelial cultures exposed to the Δ*fhs/piaA* strain were comparable in appearance to non-infected cells by SEM, exposure to the 6B WT and Δ*proABC/piaA* strains resulted in an increased abundance in secreted mucus globules compared to non-infected cells (Figure 4A).

We quantified confocal microscopy images to assess the expression of protein markers that are typical in differentiated respiratory epithelium following infection with different strains. We found a significant increase in expression of acetylated tubulin following infection with the Δ*proABC/piaA* strain (Figure 4B and 4E, left graph) and an increased expression of uteroglobin (found on Clara cells) following exposure to Δ*fhs/piaA* strain (Figure 4D and 4F, left graph). The latter also translated into a significant increase in uteroglobin positive cells within the epithelium (Figure 4F, right graph). Differential secretion of preformed mucus by the epithelium was not associated with differences in the expression of the gel-forming glycoprotein Mucin5AC following infection with the 6B WT and mutant strains (Figure 4C and 4E, right graph).

Together, these findings show that pneumococcal infection induces considerable remodelling of the epithelium which varies between infection with the different strains.

Microinvasion is not the sole determinant of the epithelial transcriptomic response to pneumococcal colonisation.

We have previously shown a broad range of host transcriptomic responses by Detroit 562 cells exposed to different pneumococcal strains including 6B (BHN418)[3]. To assess whether the enhanced microinvasion and the cellular remodelling observed with the 6B biosynthesis gene mutants alter the coordinated inflammatory response, we assessed epithelial transcriptomic profiles following pneumococcal infection by RNAseq. Compared to non-infected cells (Figure 5A), we found that all strains upregulated 78 core epithelial genes related to cytokine signalling in immune system, NLR signalling and GPCR ligand binding. 193 genes were upregulated by both the 6B WT and Δ*proABC/piaA* strains, characterised by Rhodopsin-like receptors, GPCR ligand binding, cytokine signalling in Immune system, signalling by Interleukins and Toll Receptor Cascades. Infection with the Δ*fhs/piaA* strain resulted in a markedly different transcriptomic profile with modest upregulation of 254 genes, characterised by antigen processing, proteasomal pathways, GTP hydrolysis, and intracellular stress responses (Figure 5A). Focusing on the 20 most upregulated epithelial genes

revealed again that infection with 6B WT or Δ*proABC/piaA* strain induced a similar transcriptomic profile which contrasted with that of Δ*fhs/piaA* strain which upregulated different epithelial genes at a relatively low-level induction (Figure 5B).

Transcription factors (Figure 5C), cellular kinases (Figure 5D) and cytokines (Figure 5E) bioinformatically predicted to regulate differentially expressed genes, showed the greatest difference in profile following infection with Δ*fhs/piaA* strain, with diminished NFκB and MAPK activation predicted compared to infection with 6B WT and Δ*proABC/piaA* strains. Infection with Δ*fhs/piaA* strain instead induced a more intrinsic and epithelial repair response which included TBK1, Raf1, JAK1 kinases and IL-1 and IL-33 cytokine signalling. To explore the functional consequence of cytokine activity in infected Detroit 562 cells, we also assessed the expression of validated transcriptional modules that reflect cytokine activity. This showed that 6B WT and Δ*proABC/piaA* strains induced high levels of IL-1A, IL-1B and IL-6 gene expression responses (Figure 5F).

Analysis of primary epithelial cell gene expression by RT PCR further supports our Detroit 562 pneumococcal infection data. In particular, we observed a more inflammatory profile (upregulated cytokines, chemokines, transcription factors and gene regulators) with the 6B WT and Δ*proABC/piaA* strains compared to Δ*fhs/piaA* strain, as assessed by RT PCR (Supplemental Information Figure 5).

Deletion of *proABC* and *fhs* genes influence pneumolysin activity and pneumococcal hydrogen peroxide production.

The *S. pneumoniae* pore forming toxin pneumolysin can both activate and suppress the innate immune response[15,16]. Pneumolysin also mediates the haemolytic activity characteristic of the pneumococcus[17]. We therefore hypothesised that differential expression of pneumolysin among the mutant strains may explain the differences in epithelial cell transcriptomes resulting from infection with the WT and the isogenic mutant strains. Compared to 6B WT, we observed a significant increase

in pneumolysin gene expression by the Δ*proABC* and Δ*fhs* strains following serum stress (Supplemental Information, Table 1). We also observed significant increases in haemolytic activity with the Δ*proABC* strain in a bioassay (Figure 6A). These potential differences in pneumolysin expression may partially explain differential effects on the epithelial transcriptome and cellular remodelling following infection with the mutant strains compared to WT.

Hydrogen peroxide (H_2O_2) is released by *S. pneumoniae* during infection and is regulated by enzymes encoded by such as s*pxB*, *spx* and *lctO* [18,19]. Both Δ*proABC* and Δ*fhs* strains significantly increased expression of *spxB, lctO* and *adhE* transcripts when the bacteria were cultured in serum-induced stress conditions, compared to WT (Supplementary Information Table 1). We therefore postulated that differential expression of pneumococcal H_2O_2 may modulate epithelial functional responses during colonisation of the nasopharynx. To assess this, we measured H_2O_2 concentration using a luminescence-based bioassay, normalising against bacterial CFU for each strain.

Of note, after one hour of infection, levels of hydrogen peroxide were significantly higher in bacterial cultures alone compared to bacteria in the presence of epithelial cells. The Δ*fhs/piaA* strain generated significantly more hydrogen peroxide per bacterium, across all time points, irrespective of epithelial cellular presence, compared to the 6B WT and Δ*proABC/piaA* strains (Figure 6B).

To confirm whether the source of H_2O_2 was primarily from the pneumococcus and not the epithelial cells, cells were incubated with the pneumococcal strains for 1hr and washed from non-adherent bacteria. This removed bacteria from the supernatant so that only epithelial-associated and bacteria that had microinvaded, remained. After a further 2 hours (total 3-hour timepoint) or 5 hours (total 6-hour timepoint) incubation in fresh cell media, the amount of H_2O_2 was measured. Although increased levels of H_2O_2 levels were much lower compared to those obtained when pneumococcal inoculum was present for the duration of the 3 hour infection (Figure 6B), again more H_2O_2 was detected following infection with the Δ*fhs/piaA* strain (Supplemental Information Figure 7). Hence,

altered H_2O_2 production could therefore partially explain the differential epithelial transcriptomic profile following infection with Δ*fhs/piaA* strain.

Differential caspase activity in epithelial cells following infection with the pneumococcal strains.

Production of hydrogen peroxide by the pneumococcus influences the activity of the inflammasome[20]. The NLRP3 inflammasome drives apoptosis via caspase 1 and regulates pyroptosis via caspase 3/7 activity[20]. We hypothesized that the differential microinvasion, pneumolysin activity and hydrogen peroxide production seen with the WT 6B and mutant strains would differentially influence caspase activity.

Compared to non-infected cells, infection with 6B WT and Δ*proABC/piaA* strains led to a 1.5-fold increase in epithelial caspase activity 3-hour post infection, with all strains inducing caspase activity by 6hr post infection (Figure 6C, 6D, dark grey bars). To test which caspases were activated, we incubated infected cell cultures with either a caspase 1 inhibitor (YVAD-CHO, Figure 6C, light grey bars), a caspase 3/7 inhibitor (Z-VAD-FMK, Figure 6D, light grey bars), or specifically detected caspase 8 activity (Figure 6E). The results show that at baseline, 8% of caspase activity was attributable to caspase 1 (Figure 6C). However, upon infection, we detected an increase in caspase activity in the presence of the caspase 1 inhibitor, suggesting activation of other caspases, in particular following infection with Δ*fhs/piaA* and Δ*proABC/piaA* strains. Infection with primary epithelial cells also revealed similar findings (Supplemental Information Figure 8). Next, we measured caspase 3/7 activity in cells infected with the different pneumococcal strains. In non-infected cells, 50% of caspase activity was attributable to caspase 3/7 activity, which was unaffected following 3-hour pneumococcal infection (Figure 6D). However, following 6-hour incubation with pneumococcal strains, caspase activity derived from epithelial cells infected with Δ*proABC/piaA* strain was not caspase 3/7 driven (97% activity remaining after inhibition), compared to Δfhs*/piaA*

strain (73% activity remaining after inhibition). Finally, we tested for caspase 8 activity and found a significant activation following infection with 6B WT, and to a lesser extent with Δ*proABC/piaA* strain (Figure 6E). Together, these data suggest differential caspase induction following infection with different strains, with 6B WT inducing highest caspase 8 activity and Δ*fhs/piaA* inducing the most caspase 3/7 activity.

DISCUSSION

There is considerable variation in the propensity of different *S. pneumoniae* strains to colonise the human host, cause invasive disease and transmit to others[1]. We have previously proposed that epithelial microinvasion and the subsequent inflammatory response may determine the outcome of colonisation[3], and reported that epithelial association and microinvasion profiles differ between pneumococcal strains with different capsular serotypes, and showed that these translated to unique epithelial transcriptomic and protein expression profiles[3]. As well as the capsule, *S. pneumoniae* factors affecting epithelial interactions and nasopharyngeal colonisation include multiple cell wall adhesins[1] and secreted pneumolysin[15]. In addition, *S. pneumoniae* metabolism profoundly affects systematic infection[9,21,22], and multiple bacterial metabolic pathways are also likely to influence colonisation, including those involved in DNA, protein, cell wall and fatty acid synthesis, purine and pyrimidine metabolism, and oxidative phosphorylation[23].

To investigate the role of bacterial metabolism in colonisation, we used biosynthesis pathway isogenic mutants attenuated in causing systematic disease but not for carriage, to investigate how *S. pneumoniae* metabolism affects interactions with respiratory epithelium[12]. *proABC* operon consists of three genes involved in proline biosynthesis (ProABC) and *fhs* encodes the formate tetrahydrofolate synthetase (Fhs) which catalyses the synthesis of N10 formyl tetrahydrofolate, crucial for carbon metabolism and purine nucleotide biosynthesis in a number of bacterial species[24,25]. The function of the Fhs is thought to be particularly relevant in hypoxic conditions[25,26] and mutations in *fhs* gene have also been linked to increased antimicrobial resistance[27,28]. Although

a piaA mutation was added to ensure attenuation in the EHPC model, we found no evidence that this influenced the outcome of epithelial infection. We now show that alterations in pneumococcal metabolism caused by deletion of *fhs* or *proABC* have profound effects on *S. pneumoniae* under stress conditions. This translates to diverse effects on respiratory epithelial association, microinvasion, transmigration, the subsequent epithelial inflammatory response, cellular re-modelling and caspase activation. We implicate differences in pneumolysin expression and activity, and regulators of pneumococcal oxidative stress that impacts on hydrogen peroxide secretion in these epithelial processes. These data highlight the complex downstream effects of bacterial metabolism and indicate that epithelial microinvasion by *S. pneumoniae* may result in a multitude of host cellular and bacterial outcomes (Graphical Abstract). Indeed, these findings add weight to our proposition that adaptation to microinvasion by the pneumococcus may both facilitate immune evasion and, as is typical of 'professional' intracellular bacterial species such as *Listeria* and *Salmonella*, trigger inflammation to ultimately mediate transmission[29,30].

Using a well-characterised primary epithelial cell model[31], we found that *S. pneumoniae* interacts with each of the constituent epithelial subtypes: Clara cells (secretory, xenobiotic metabolic, and progenitor cell functions), goblet cells (mucus production), ciliated cells (mucus and small particle transport). The apparent downstream effects of infection with these biosynthesis mutants on epithelial biology following microinvasion varied considerably. The intensity of β catenin, an adherens junction protein, increased at the epithelial junctional membrane following infection with the Δ*proABC/piaA* strain. We saw an enrichment of goblet cell pre-formed mucus release following infection with 6B WT and Δ*proABC/piaA* strain but not the Δ*fhs/piaA* strain, although with no corresponding detectable effects on Muc5AC glycoprotein expression. We also identified increased staining for acetylated tubulin (marker of ciliated cells) with Δ*proABC/piaA* exposure and enrichment of staining for uteroglobin (marker of clara cells) with Δ*fhs/piaA* exposure. In a rabbit meningitis model, increased acetylated tubulin and microtubule stabilisation was attributed to pneumolysin activity[32], suggesting the increase in pneumolysin activity with Δ*proABC/piaA* strain could contribute to our observed changed in cellular remodelling.

We speculate that this cellular remodelling could enhance barrier function, modulate permissiveness to bacterial microinvasion and impact on bacterial clearance. Importantly, the differential epithelial effects following infection with the different strains appears not to relate to bacterial load and intracellular survival potential, but instead is more closely linked to differences in pneumococcal metabolic and virulence factor adaptations to stress that are independent of capsule serotype.

Infection with either the 6B WT or Δ*proABC/piaA* strain induced innate inflammatory pathways typical pneumococcal infection[3], including those related to cytokine/chemokines, interleukins, Toll Like Receptor and NFκB signalling, together with apoptotic transcripts such as FOXO3 and TP53. We also identified epithelial genes that were increased only following WT infection, including RNA degradation and O-linked glycosylation that resulted in increased gene expression involved in wnt (which may be linked to the increase βcatenin expression we observed[33]), DNA sensing, RIG-I pathways and signal transduction. In contrast, the Δ*fhs/piaA* strain appeared to activate an epithelial pro-survival and adaptation profile which included JUN, SMARCA4, NFAT5, KLF6 and TCF4 genes involved in homeostatic signalling and chromatin remodelling[34,35]. These illustrate the multifaceted outcomes of epithelium microinvasion with the potential for either an inflammatory or a more tolerant response. Whether this translates to differences in the length of nasopharyngeal carriage, invasiveness or clearance of the pneumococcal remains to be fully determined, but in the EHPC model, increased density of the Δ*fhs/piaA* strain was seen at day 6 post-inoculation compared the other strains[11]. Ultimately, these epithelial transcriptomic differences may also shape the adaptive immune response to pneumococcal colonisation[14,36], which could also influence disease outcome.

S. pneumoniae is a catalase-negative, facultative anaerobe intrinsically resistant to hydrogen peroxide (H_2O_2) which is produced endogenously by pyruvate oxidase (*SpxB*) and acetate oxidase (*LctO*) particularly under conditions of aerobic growth[18,19,37]. We found enriched transcripts for *SpxB* and *LctO* in the isogenic mutants, under stress conditions, which suggests a switch in metabolism

and may explain differences observed in epithelial adherence compared to 6B WT[6]. Although, *SpxB* is not crucial for pneumococcal disease[38], H_2O_2 production is a potent virulence factor, limiting the growth of a variety of competing organisms in the upper respiratory tract, inducing host cell endoplasmic reticulum stress, and is an intracellular signalling molecule that has been shown to modulate inflammation, glycolytic flux, pyruvate metabolism, nucleotide biosynthesis, and capsule biosynthesis[6,39]. We have shown that deletion of *proABC* or *fhs* genes impact on pneumococcal oxidative stress regulation, which may contribute to epithelial remodelling, induction of caspase activity and the epithelial transcriptomic response to infection. Although hydrogen peroxide induces DNA damage and apoptosis of the lung epithelium[20,40], pneumococcal-derived hydrogen peroxide has been shown to regulate host responses via inhibition of inflammasome activation[18]. Indeed, we did not detect significant caspase 1 activity following infection. In our models, we provide evidence to suggest that caspases 3/7 and 8 are activated following infection with Δ*fhs/piaA* strain and 6B WT respectively, which may have downstream implications in chromatin condensation, DNA repair and alarmin release[41].

S. pneumoniae is highly adapted to colonise the human host and be transmitted from person to person. Invasive pneumococcal disease, particularly in it severest forms is largely a dead end for the bacteria. The data presented here further support our hypothesis that epithelial microinvasion in healthy people is frequent and mostly does not lead to disease. However, the subsequent epithelial-derived innate responses to microinvasion are likely influenced by a range of bacterial metabolic and virulence factors. Our findings highlight the broad-ranging effects of single gene mutations in pneumococcal biosynthesis pathways which may in part, explain the complexity of the differences between even seemingly closely related pneumococcal strains.

METHODS

Bacteria

The Streptococcus pneumoniae serotype 6B (strain BHN 418[42]) was a kind gift from Prof. Birgitta Henriques Normark (Karolinska Institute). Δ*proABC/piaA* and Δ*fhs/piaA* mutant strains were generated using overlap extension PCR as described by Ramos-Sevillano et al[12]. Stocks of bacteria were stored at -80ºC when bacterial growth in Todd Hewitt Broth (THY) was 0.3 $O.D._{600nm}$. Aliquots were defrosted, centrifuged at 8000g for eight minutes and resuspended in 1% Fetal Bovine Serum (FBS, Gibco) in MEM media (Gibco) for infections. Approximately 10 bacteria were added for every epithelial cell. Colony forming units (CFU) were counted by serial dilutions on horse blood agar plates (EO Labs). Starting inoculums were not significantly different across strains for all assays.

Bacterial RNA-seq sample collection, sequencing and reads

Mutant pneumococcal strains (three biological replicates for each mutant) and 6B WT (three biological replicates) were grown in THY to mid log phase and the pellets resuspended in THY and undiluted human serum for 60mins. The culture was then pelleted, and RNA stored in RNA Protect at -70ºC before extracting total RNA[13]. Total RNA from each library was ribo-depleted and sent for Illumina Next Seq Sequencing Pathogen Genomics Unit (PGU), UCL. The quality of raw FASTQ reads was checked by FastQC v0.11.5, Babraham Bioinformatics, UK[43] and visualised using multiQC v1.9[44]. Reads were trimmed using Trimmomatic 0.39[45]. Trimmed reads were also checked by FastQC and multiQC. Trimmed reads were then mapped to KEGG annotated 6B genome sequence (670-6B, Accession: CP002176.1) using bowtie2 with default settings[46]. Conversion into BAM files was performed using SAMtools[47]. Mapped reads were visualized in the Integrated Genome Browser (IGB)[48]. FeatureCounts v2.0.0 was used to summarize read counts for each annotated feature in the respective reference genomes in multimapping mode (-M)[49].

Differential gene expression analyses

The generated count matrix was imported into R-studio (R v3.4.2) and normalization of counts and differential gene expression analysis was performed by DESeq2[50]. DESeq2 normalized libraries were regularized log transformed for visualizing heatmaps and clustering. Differential gene

expression was performed on raw counts. Fold change shrinkage was implemented with the apeglm package within DESeq2. Genes with a log2 fold change > 1.5 and false discovery rate (FDR) of < 0.05 were categorized as differentially expressed. KEGG pathway enrichment and module analysis were performed on differentially regulated genes using over representation analysis (ORA) implemented by clusterProfiler[51].

Experimental Human Pneumococcal Carriage Model (EHPC)

A full explanation of experimental design and selection criteria has been previously described[3]. Following written informed consent, healthy non-smoking adults between the ages of 18 – 59 were inoculated with 80,000 CFU/nostril live strains of *S. pneumoniae*. Mucosal cells from the inferior turbinate using a plastic Rhino-probe™ (curettage, Arlington Scientific) were collected prior to inoculation, and days 2 and 6 post-inoculation. Samples were processed for confocal microscopy analysis. Nasal wash samples were collected for CFU count analysis. There were no adverse events. Ethical approval was given by NHS Research and Ethics Committee (REC)/Liverpool School of Tropical Medicine (LSTM) REC, reference number: 18/NW/0481 and Human Tissue Authority licensing number 12548.

Primary Human Epithelial Cells

Normal Human Primary Bronchial/Tracheal Epithelial Cells (NHBE-A, ATCC® PCS-300-010™) were plated at $6x10^3$ cells/cm^2 on a layer of sub-lethally γ-irradiated (60 Gy) mouse embryonic fibroblasts 3T3-J2 cells (kind donation from Howard Green, Harvard Medical School, Boston[52]) with keratinocyte culture medium cFAD (3:1 DMEM (Gibco) to Ham F-12 Nut Mix (Gibco), 10% FBS (HyClone, Sigma), 1% Penicillin-Streptomycin (100X, Sigma), 0.4 µg/mL Hydrocortisone (Calbiochem, USA), 5 µg/ml Insulin (various), 10-10 Cholera Toxin (Sigma) and 2x10-9 Triodothyronine (Sigma)). Epithelial cells were stimulated with 10 ng/mL human epidermal growth factor (hEGF, PeproTech, USA) on days 3 and 5. Cultures were grown at 37ºC 6% CO_2 and sub-confluent cultures were trypsinised with 0.25% Trypsin-EDTA (Sigma). For NHBE-A differentiation in Air Liquid Interface (ALI) culture, cells were

plated at a density of $6x10^4/cm^2$ on 1µm pore PET cell culture inserts (12 wells, Greiner). The insert was supplemented with cFAD medium on the top and bottom. After 48 hours, medium was removed from the top of the culture (exposure) and the culture was fed with fresh PneumaCult™ differentiation Medium (Stemcell Technologies) from the bottom of the well every 2 days for 3 weeks, until cell ciliation was observed. Antibiotics were removed from the medium and cells washed 24 hours before infection experiments.

Human Epithelial Cell Lines

Human pharyngeal carcinoma Detroit 562 epithelial cells (ATCC_CCL-138) were grown in 10% FCS in alpha MEM media (Gibco). For each set of experiments, cells were used within 5 passages. Cells consistently tested PCR negative for mycoplasma (Cambridge Biosciences).

Pneumococcal-epithelial cell co-culture

For association and internalisation assays, confluent monolayers of Detroit 562 cells (typically day 7 - 8 post plating) cultured on 12 well plates (Corning), were exposed to *S. pneumoniae* (1 cell : 10 pneumococci) for three hours in 1% FCS alpha MEM (six-hour infection for HNBE-A cells in 1% Pneumocult media without supplements)[3]. Cells washed three times in $HBSS^{+/+}$ before incubation in 1% saponin for 10 minutes at 37°C to lyse cells. Bacterial dilutions were plated on horse blood agar for 16 hours and colony forming units counted. For internalisation quantification, 200µg/ml gentamicin was added to the cells for one hour before incubation with saponin.

For transmigration assays, Detroit 562 cells were plated onto 3µm pore, PET Transwell Inserts (ThermoFisher) typically for 10 days[3]. Media was changed to 1% FCS (250µl apical chamber, 1ml basal chamber) one hour prior to infection experiments. 1mg/ml FITC-dextran (Sigma Aldrich) was added to the apical chamber of selected inserts for permeability assays. Transepithelial Electrical Resistance (TEER) was measured before and after infection using an EVOM2 (World Precision Instruments). Bacteria were added to the cells for three hours during of which 50µl of basal media

was repeatedly removed to measure bacterial load by counting CFU/well. Permeability was recorded using a FLUOstar Omega (BMG Labtech) at 488nm.

Confocal Microscopy

Sample processing was performed as previously described[3]. Briefly, mucosal cells from the EHPC model were placed directly into 4% PFA and cytospun onto microscope slides. NHBE-A cells and Detroit 562 cells cultured on transwell membranes were fixed in 4% PFA (Pierce, Methanol Free). Cells were permeabilised with 0.2% Triton X-100 for 10 minutes, blocked for one hour in blocking buffer (3% goat serum and 3% BSA in PBS (Sigma)) and incubated with pneumococcal antisera Pool Q (SSI Diagnostica) for one hour. Wheat germ agglutinin conjugated to Rhodamine (Vector Labs) was added along with goat-anti rabbit IgG conjugated to Alexa Fluor 488 for 45 minutes in blocking buffer. Primary (used at 1:100) antibodies used for epithelial cell proteins can be found in Supplemental Information Table 3. Secondary (used at 1:500) antibodies were either goat anti-mouse or goat anti-rabbit – Alexa Fluor 555 or 546, ThermoFisher. Of note, for epithelial protein antibodies raised in rabbit, no pneumococcal staining was possible and therefore pneumococci were not visible on the images (uteroglobin). DAPI was added for 5 minutes and cells were mounted with Aqua PolyMount (VWR International) and a coverslip on the microslide. Pneumococci were recorded by manual scanning of the whole cytospin for the EHPC samples. More than three fields of view were recorded for each bacterial strain for Detroit 562 cell infections, using inverted Zeiss LSM (either 700 or 880) confocal microscopes. Images were processed with Zeiss LSM Image Browser. Z stacks were recorded at 1µm intervals at either 40x oil or 63x oil objectives. Automated image analysis was carried out using Cellprofiler[53].

Electron Microscopy

Preparation of Detroit 562 cells and NHBE-A cells was identical, and previously described[3]. Briefly, cells cultured on transwells were fixed with 2% paraformaldehyde and 1.5% glutaraldehyde in 0.1 M cacodylate buffer and post-fixed in 1% OsO4 / 1.5% K4Fe(CN)6 in 0.1 M cacodylate buffer pH7.3. Samples were dehydrated in graded ethanol-water series and infiltrated with Agar 100 resin mix.

Ultra-thin sections were cut at 70-80 nm using a diamond knife on a Reichert ultracut microtome. Sections were collected on 300 mesh copper grids and stained with lead citrate. For transmission electron microscopy the samples were hardened at 60ºC for 48 hours. The coverslip was removed, and a representative area was selected. Ultra-thin sections were cut at 70-80 nm using a diamond knife on a Reichert ultra-cut S microtome. Sections were collected on copper grids and stained with lead citrate. Samples were viewed with a Joel 1010 transition electron microscope and the images recorded using a Gatan Orius CCD camera.

Pneumolysin activity

Adapted from Kirkham et al[54]. Briefly, final concentration of 2% horse blood (EO Labs) solution was prepared in phenol free alpha MEM (Life Technologies) and 100 µl added to wells of a 96 U-bottom plate (Corning). 100 µl of bacterial solutions (containing ~2.5×10^6 bacteria) were suspended in phenol free alpha MEM were added to each 96 well. Saponin was used as a positive control for lysis. Solutions were incubated for 30 minutes at 37ºC before centrifugation at 1000g for one minute. 100 µl was transferred into a new 96 well plate and absorbance recorded at 540nm on a plate reader.

Hydrogen Peroxide Assay

Detroit 562 cells were cultured in white 96 well plates (Corning). NHBE-A cells were cultured in 12 well plates in Pneumocult media. Cells were incubated with H_2O_2 substrate and infected with strains of *S. pneumoniae* for up to six hours according to manufacturers' instructions (ROS-Glo™ H_2O_2 Assay, Promega). ROS-Glo™ Detection solution was added to the cells and incubated for 20 minutes. For primary cells, supernatant was then transferred to a white 96 well plate. Luminescence was read using a GloMax -Multi Detection System plate reader (Promega).

Lactate Dehydrogenase Assay

Detroit 562 cells and NHBE-A cells were cultured in 12 well plates and infected with pneumococcal strains for six hours. Supernatant was centrifuged at 8000g for 8 minutes and pellet discarded. Supernatant was transferred to a clear 96 well plate (Corning) and CytoTox 96® Reagent was added for 30 minutes according to manufacturers' instructions (CytoTox 96® Non-Radioactive Cytotoxicity

Assay, Promega). After adding Stop Solution, absorbance was measured at 490nm using a plate reader. % Cytotoxicity was calculated using the following equation: 100 x (LDH release – background from media alone)/(max LDH release from positive control – background from media alone).

Caspase assay

Detroit 562 cells were cultured in white 96 well plates (Corning). NHBE-A cells were cultured in 12 well plates in Pneumocult media. Cells were infected with strains of *S. pneumoniae* for up to six hours. Primary cell supernatant was transferred to a white 96 well plate. Samples were incubated with Caspase-Glo® 1 Reagent, Caspase-Glo® 1 YVAD-CHO Reagent, Caspase-Glo® Z-VAD-FMK Reagent or Caspase-Glo® 8 Reagent, for one hour and according to manufacturers' instructions (Promega). Luminescence was read using a GloMax-Multi Detection System plate reader (Promega).

RNA samples and sequencing (RNA-Seq)

RNA-Seq data was collected as previously described[3]. Confluent monolayers of Detroit 562 epithelial cells were infected with *S. pneumoniae* strains for four hours before collection in RNALater. RNA was extracted using a Qiagen RNAEasy micro kit and treated for DNA removal using a Qiagen Turbo DNA-free kit. RNA quality was assessed and quantified using a BioAnalyser (Agilent 2100). Samples were sequenced using Illumina Nextseq 500/550 High Output 75 cycle kit giving 15-20 million 41bp paired-end reads per sample (Pathogens Genomic Unit, UCL).

Statistics

Each condition within each experiment was performed in duplicate or triplicate, and each experiment was performed independently more than three times, unless stated otherwise. Error bars represent SEM, unless stated otherwise. GraphPad Prism Version 7 was used for parametric (t-tests or ANOVA) or non-parametric (Mann-Whitney or Kruskal-Wallis tests) analysis, which was based on the Shapiro-Wilk normality test. Ad hoc tests were performed using Tukey's (for parametric data) or

Dunn's (for non-parametric data) multiple comparisons test. P values less than 0.05 were considered significant.

Data and code availability

Source data are provided as a Source Data file. RNAseq data from the Detroit 562 cell infections is publicly accessible through Zenodo with Accession (DOI:10.5281/zenodo.7997789).

ACKNOWLEDGEMENTS

This study was funded by CMW from a Postdoctoral Innovation Award from UCL, a Pump-Priming Award and Enhancement Award from the Human Infection Challenge Network for Vaccine Development (HIC-VAC (funded by the GCRF Networks in Vaccines Research and Development) which is co-funded by the MRC and BBSRC). This UK funded award is part of the EDCTP2 programme supported by the European Union. CMW and RSH are supported by the Medical Research Council (grant MR/T016329/1). The authors would like to thank Prof. Peter Hermans (Radboud University Medical Centre) for donating the 6B pneumococcal strain originally from Prof. Birgitta Henriques-Normark (Karolinska Institute) and obtained directly from DF at LSTM. EHPC sample collection was supported by the Medical Research Council (grant MR/M011569/1), Bill and Melinda Gates Foundation (grant OPP1117728) awarded to DF and the National Institute for Health Research (NIHR) Local Comprehensive Research Network. The authors also wish to thank the EHPC Clinical Team at LSTM and all the volunteers. Confocal imaging facilities at LSTM were funded by a Wellcome Trust Multi-User Equipment Grant (104936/Z/14/Z). Electron microscopy processing and image capture was performed by Dr. Elizabeth Slavik-Smith in the Biosciences EM facility at UCL. MC is supported by a Springboard to Independence grant (AirwayStasis) from the French Government's Investissement d'Avenir program, the Laboratoire d'Excellence ''Integrative Biology of Emerging Infectious Diseases" (ANR-10-LABX-62-IBEID) and the Chromatin and infection unit headed by Melanie A. Hamon. RNA-Seq library preparation was undertaken at UCL through the UCL/UCLH Biomedical Research Centre and MRC funded Pathogen Genomics Unit (PGU,

G0900950). All RNAseq data processing was completed by the PGU. MN is supported by the Wellcome Trust and by NIHR Biomedical Research Centre Funding to University College Hospitals NHS Foundation Trust and University College London. RR is supported by Marie Skłodowska-Curie Individual Fellowships 896014. PB is supported by the European Research Council (ERC-Stg No. 639429), the Rosetrees Trust (M362-F1; M553), the CF Trust (SRC006;SRC020), the London Advanced Therapies - Research England (C2N-AT.006), the MRC Confidence in Concept scheme (Award: MC_PC_17180), the Innovate UK (Smart grant n.10005465), the Duchenne Parent Project (DPP) and the NIHR GOSH BRC. MW is supported by a 223065 Wellcome Investigator Award to CJ. ERS and JSB are supported by MRC grant R/N02687X/1 and Wellcome grant 221803/Z/20/Z. JSB is partially supported by the Department of Health's National Institute of Health and Care Research Biomedical Research Centre funding to UCLH. RSH is a NIHR Senior Investigator.

AUTHOR CONTRIBUTIONS: CMW conceived, funded, designed and conducted the study, performed the experiments, acquired samples and processed data, and wrote the first draft of the manuscript. GP analysed and interpreted the RNAseq data. MB analysed and interpreted the bacterial transcriptomic data. RR cultured and differentiated primary epithelial cells. MC ran the primary cell qPCR. ERS generated the mutant strains and bacterial transcriptomic data. JR collected and processed EHPC samples. JAGA processed the RNA-Seq data. MW ran the image analysis. PB and CJ provided investigator support. MN provided RNA-Seq analysis support. DF provided investigator support and EHPC clinical samples. JSB generated the mutant strains, interpreted the data and revised the manuscript. RSH provided investigator support, designed and interpreted the data, revised the manuscript. All authors commented on and approved the manuscript.

COMPETING INTERESTS: The authors declare no competing interests.

FIGURE LEGENDS

Table 1. Differentially expressed pathways from single isogenic mutants in human serum compared to WT. 55 genes were selected within competence pathways, amino acid metabolism, virulence factors, oxidative stress pathways and other known genes important for colonisation, for assessment of changes in gene expression following serum stress.

Figure 1. Pneumococcal – epithelial interactions in the EHPC model. (A) During colonisation, pneumococci adhere to the epithelial cell surface (Association), internalise inside epithelial cells (Microinvasion) and movement (transmigration) across the epithelial barrier. Mucus – lime; pneumococci – purple; intracellular vacuole – dark green; epithelial cells – yellow; nucleus – brown; cell junctions – pink. (B) Representative microscopy images showing 6B association to the epithelium and mutant microinvasion. Surface carbohydrates (red), nuclei (DAPI, blue), pneumococci (green). (C) Mucosal curettage samples were collected at day 6 post-pneumococcal challenge. Percentage of bacteria that were found by microscopy, on the surface (association) or inside (microinvasion) cells in the EHPC model. Number of volunteers (n) in each group is indicated in brackets, along with the total numbers of pneumococci (Spn) counted. (D) Micro-invasive index per volunteer, calculated from microscopy counts, for each strain. p = 0.1701, Kruskal-Wallis.

Figure 2. **Strain association, microinvasion and transmigration of Detroit 562 cells.** Cells were infected with *S. pneumoniae* for three hours and CFU counts recorded. (A) Representative confocal microscopy images from 6 independent experiments with replicates, showing pneumococcal (green) interactions with surface carbohydrates (red). (B) Association of pneumococcal strains to epithelial cells. p = 0.0009 (Kruskal-Wallis), n = 6 with replicates. (C) Internalisation of strains into cells. p = 0.0219 (Kruskal-Wallis) N = 6 with replicates. (D) Microinvasive index is defined as the percentage of internalised bacteria over all associated bacteria. p = 0.071 (Kruskal-Wallis) N = 6 with replicates. (E) Pneumococcal viability inside epithelial cells. n = 3 or 4 independent experiments with replicates. Counts were normalised to microinvasion counts for each strain after 3 hours infection and compared to 6B WT; +1hr p = 0.6517, +2hr p = 0.1377, +3hr p = 0.1183 (ANOVA). (F) Transmigration of pneumococcal strains across confluent monolayers on transwell inserts. CFUs were recorded from

the basal chamber. N = 6 independent experiments with replicates. $p < 0.001$ (Kruskal-Wallis). (G) Epithelial cell permeability was assessed via leak to 4kDa FITC-Dextran into the basal chamber. N = 4 with replicates. $p < 0.0001$ compared to non-infected cells, and $p = 0.0689$ between 6B WT and mutant strains (Kruskal-Wallis). (H) Representative confocal microscopy images from 6 independent experiments with replicates, showing pneumococcal (green) interactions with β catenin (red). Nuclear DAPI stain (blue). (I) Image quantification of integrated intensity of β catenin normalised to non-infected cells, following infection with the different strains. N = 5 independent experiments. Non infected v pneumococcal negative cells **** $p < 0.0001$ (NI v Δ*fhs/piaA*); non-infected v pneumococcal positive cells; **** $p < 0.0001$ (NI v 6B), * $p = 0.0183$ (NI v Δ*proABC/piaA*), * $p = 0.0149$ (NI v Δ*fhs/piaA*); Kruskal-Wallis. (J) Cell supernatant from infected cells was analysed for lactate dehydrogenase secretion. N = 3 - 5 with replicates. $p = 0.046$ compared to non-infected cells, and $p = 0.5649$ between 6B WT and mutant strains (ANOVA).

Figure 3. Effects on epithelial barrier from pneumococcal infection in HBE-A cells. Cells were cultured at ALI and infected with pneumococcal strains for 6hrs. (A) Top: Representative confocal microscopy images from 4 independent experiments with replicates, showing pneumococcal (green) association with the epithelium (red, surface carbohydrates; nuclei blue) at 6hr post infection. Bottom: Representative transmission electron microscopy images from 2 independent experiments, showing pneumococcal microinvasion examples of each strain (arrows), enclosed within a vacuole after 4hr infection. (B) Representative confocal microscopy images from 4 independent experiments with replicates, showing pneumococcal (green) interactions with junctional proteins (red) of β catenin. Colocalization of red and green appears yellow. Nuclei (blue). (C) Integrated intensity of β catenin in pneumococcal negative (not pneumococcal associated) or positive (pneumococcal associated) cells. Non infected v pneumococcal negative cells **** $p < 0.0001$ (NI v Δ*proABC/piaA*), ** $p = 0.0026$ (NI v Δ*fhs/piaA*); non-infected v pneumococcal positive cells; **** $p < 0.0001$ (NI v Δ*proABC/piaA* and NI v Δ*fhs/piaA*); Kruskal-Wallis, n = 4 independent experiments. (D) Transepithelial electrical resistance (TEER) was recorded pre- and post- 6hr infection to assess barrier integrity. N = 3 independent experiments with replicates. Average TEER pre-infection was

466Ω.cm^2 (430-484 Ω.cm^2, p = 0.1458 ANOVA) and average TEER post-infection was 545Ω.cm^2 (527-567 Ω.cm^2. p = 0.04744 ANOVA). Change in TEER comparing non-infected cells to infected cells p = 0.6592, Kruskal-Wallis. Error bars represent SEM. (E) After 6hrs infection, supernatant was collected and analysed for lactate dehydrogenase secretion from the apical and basal chamber. Non-infected v infected; p >0.05, ANOVA. N = 5-6 independent experiments with replicates.

Figure 4. Pneumococcal – epithelial interactions with primary human epithelial cells. Cells were cultured at ALI and infected with pneumococcal strains for 6hrs. (A) Representative scanning electron microscopy images from 2 independent experiments, showing the surface of the epithelium. Examples of differentiated epithelia (basal cells, clara cells, goblet cells, ciliated cells) are shown in yellow text. Examples of pneumococci are highlighted by arrows. Representative confocal microscopy images from 4 independent experiments with replicates for (B) ciliated cells (acetylated tubulin, red), (C) goblet cells (mucin5ac, red, (arrows indicate co-localisation of mucin5ac with pneumococci)), (D) clara cells (uteroglobin, red) after 6hr infection. Pneumococci (green), nuclei (DAPI, blue), colocalization of red and green appears as yellow. (E) Integrated intensity of acetylated tubulin and Muc5ac in pneumococcal negative or positive cells. Acetylated tubulin, neg p = 0.2677, pos p = 0.017; Mucin5ac, neg p = 0.6852, pos p = 0.8510, ANOVA. N = 3 or 4 independent experiments. (F) Integrated intensity of uteroglobin normalised to non-infected cells (left, p = 0.0115 non-infected v infected, Kruskal-Wallis) and percentage of clara positive cells following infection (right, p = 0.0003 non-infected v strains, p = 0.0036 6B v mutant strains, Kruskal-Wallis). N = 3 independent experiments.

Figure 5. Detroit 562 cell transcriptomic responses to pneumococcal strains. Epithelial cells were infected for four hours with pneumococcal strains and RNA extracted and processed for RNAseq. 6B n = 11, PP n = 17, FP n = 14, non-infected n = 12, from 6 independent experiments. (A) All significantly log2 fold change upregulated genes according to strain compared to non-infected cells. Significance was defined as DEGs with a log2 fold change (logFC) of > 1.5 and false discovery

rate (FDR) of < 0.05. (B) Comparison of the top 20 most upregulated genes for each strain, compared to non-infected cells. Upstream regulator analysis for (C) transcription factors, (D) kinases and (E) cytokines. (F) The expression of gene modules is represented by the mean Log_2 TPM value of the genes in each module.

Figure 6. Pneumolysin activity and hydrogen peroxide secretion from pneumococcal strains in the absence and presence of Detroit 562 cells and caspase activity in Detroit 562 cells (A) Pneumolysin activity was assessed using a red blood cell lysis assay. Strains were incubated with red blood cells for 30 minutes and absorbance measured. N = 4 experiments with replicates. Pneumococcal strain haemolytic activity is calculated in comparison to 100% lysis by 0.0625% saponin. p <0.0001 compared to 6B wild type (ANOVA). (B) Fold change of hydrogen peroxide production from the mutants compared to WT, normalised to the CFU counts. Without cells (dark grey) 1h p = 0.0369 (ANOVA), 3hr p = 0.0087 (ANOVA), 6hr p = 0.0209 (Kruskal-Wallis). With Detroit 562 cells (light grey), 1h p = 0.2170 (ANOVA), 3hr p = 0.0281 (ANOVA), 6hr p = 0.0243 (Kruskal-Wallis). Caspase activity was assessed by luminescence, following infection with pneumococcal strains. (C) Caspase 1 activity was determined following incubation with the specific inhibitor YVAD-CHO. N = 6 with replicates. In comparison to non-infected cells, 3hr caspase p = 0.0297; caspase+YVAD-CHO inhibitor p = 0.0479 and, in comparison to 6B WT, 3hr caspase p = 0.0173; caspase+YVAD-CHO inhibitor p = 0.5725 (Kruskal-Wallis). In comparison to non-infected cells, 6hr caspase p = 0.39; caspase+YVAD-CHO inhibitor p = 0.3604 and, in comparison to 6B WT, 6hr caspase p = 0.6226; caspase+YVAD-CHO inhibitor p = 0.5386 (Kruskal-Wallis). (D) Caspase 3/7 activity was determined following incubation with the specific inhibitor Z-VAD-FMK. N = 4 with replicates. In comparison to non-infected cells, 3hr caspase p = 0.0001; caspase+Z-VAD-FMK inhibitor p = 0.0165 and, in comparison to 6B WT, 3hr caspase p = 0.0036; caspase+ Z-VAD-FMK inhibitor p = 0.0036 (Kruskal-Wallis). In comparison to non-infected cells, 6hr caspase p = 0.0022; caspase+ Z-VAD-FMK inhibitor p = 0.0005 and, in comparison to 6B WT, 6hr caspase p = 0.0215; caspase+ Z-VAD-FMK inhibitor p = 0.0012 (Kruskal-Wallis). (E) Caspase 8 activity was assessed

following infection with pneumococcal strains. N = 3 with replicates. In comparison to non-infected cells, 6hr $p = 0.0015$ (ANOVA) and, in comparison to 6B WT, $p = 0.0172$ (ANOVA).

REFERENCES

1 Weiser, J. N., Ferreira, D. M. & Paton, J. C. Streptococcus pneumoniae: transmission, colonization and invasion. *Nat Rev Microbiol* **16**, 355-367, doi:10.1038/s41579-018-0001-8 (2018).

2 O'Brien, K. L. *et al.* Burden of disease caused by Streptococcus pneumoniae in children younger than 5 years: global estimates. *Lancet* **374**, 893-902, doi:10.1016/S0140-6736(09)61204-6 (2009).

3 Weight, C. M. *et al.* Microinvasion by Streptococcus pneumoniae induces epithelial innate immunity during colonisation at the human mucosal surface. *Nat Commun* **10**, 3060, doi:10.1038/s41467-019-11005-2 (2019).

4 Gladstone, R. A. *et al.* International genomic definition of pneumococcal lineages, to contextualise disease, antibiotic resistance and vaccine impact. *EBioMedicine* **43**, 338-346, doi:10.1016/j.ebiom.2019.04.021 (2019).

5 Amin-Chowdhury, Z. *et al.* Characteristics of Invasive Pneumococcal Disease Caused by Emerging Serotypes After the Introduction of the 13-Valent Pneumococcal Conjugate Vaccine in England: A Prospective Observational Cohort Study, 2014-2018. *Clin Infect Dis* **71**, e235-e243, doi:10.1093/cid/ciaa043 (2020).

6 Echlin, H., Frank, M., Rock, C. & Rosch, J. W. Role of the pyruvate metabolic network on carbohydrate metabolism and virulence in Streptococcus pneumoniae. *Mol Microbiol* **114**, 536-552, doi:10.1111/mmi.14557 (2020).

7 Hartel, T. *et al.* Characterization of central carbon metabolism of Streptococcus pneumoniae by isotopologue profiling. *J Biol Chem* **287**, 4260-4274, doi:10.1074/jbc.M111.304311 (2012).

8 Henriques-Normark, B. & Tuomanen, E. I. The pneumococcus: epidemiology, microbiology, and pathogenesis. *Cold Spring Harb Perspect Med* **3**, doi:10.1101/cshperspect.a010215 (2013).

9 Kohler, S., Voss, F., Gomez Mejia, A., Brown, J. S. & Hammerschmidt, S. Pneumococcal lipoproteins involved in bacterial fitness, virulence, and immune evasion. *FEBS Lett* **590**, 3820-3839, doi:10.1002/1873-3468.12352 (2016).

10 Brown, J. S., Gilliland, S. M. & Holden, D. W. A Streptococcus pneumoniae pathogenicity island encoding an ABC transporter involved in iron uptake and virulence. *Mol Microbiol* **40**, 572-585, doi:10.1046/j.1365-2958.2001.02414.x (2001).

11 Hill H, M. E., Nikolaou E, Blizard A, Pojar S, Howard A, Hyder-Wright A, Devin J, Reiné J, Robinson R, Solórzano C, Jochems S, Kenny-Nyazika T, Ramos-Sevillano E, Weight CM, Myerscough C, McLennan D, MortonB , Gibbons E, Farrar M, Randles V, Burhan H, Chen T, Shandling AD, Campo JJ, Heyderman RS, Gordon SB, Brown JS, Collins AM, Ferreira DM. A Randomised Controlled Trial of Nasal Immunisation with Live Virulence Attenuated Streptococcus pneumoniae Strains using Human Infection Challenge. *Medrxiv*, doi:https://doi.org/10.1101/2023.04.14.23288224 (2023).

12 Ramos-Sevillano, E. *et al.* Preclinical Development of Virulence Attenuated Streptococcus pneumoniae Strains Able to Enhance Protective Immunity Against Pneumococcal Infection. *Am J Respir Crit Care Med*, doi:10.1164/rccm.202011-4161LE (2020).

13 Ramos-Sevillano E., E. G., Guerra-Assunção J.F., Betts M., Partridge F., Fernandes V.E., Wall E., Gordon S.B., Ferreira D.M., Heyderman R.S., Brown J.S. Essential role of proline synthesis and the one-carbon metabolism pathways for systemic virulence of Streptococcus pneumoniae. *Biorxiv*, doi:https://doi.org/10.1101/2023.08.03.550501 (2023).

14 Ferreira, D. M. *et al.* Controlled human infection and rechallenge with Streptococcus pneumoniae reveals the protective efficacy of carriage in healthy adults. *Am J Respir Crit Care Med* **187**, 855-864, doi:10.1164/rccm.201212-2277OC (2013).

15 Zafar, M. A., Wang, Y., Hamaguchi, S. & Weiser, J. N. Host-to-Host Transmission of Streptococcus pneumoniae Is Driven by Its Inflammatory Toxin, Pneumolysin. *Cell Host Microbe* **21**, 73-83, doi:10.1016/j.chom.2016.12.005 (2017).
16 Periselneris, J. *et al.* Pneumolysin suppresses the initial macrophage pro-inflammatory response to Streptococcus pneumoniae. *Immunology* **167**, 413-427, doi:10.1111/imm.13546 (2022).
17 Terra, V. S., Plumptre, C. D., Wall, E. C., Brown, J. S. & Wren, B. W. Construction of a pneumolysin deficient mutant in streptococcus pneumoniae serotype 1 strain 519/43 and phenotypic characterisation. *Microb Pathog* **141**, 103999, doi:10.1016/j.micpath.2020.103999 (2020).
18 Erttmann, S. F. & Gekara, N. O. Hydrogen peroxide release by bacteria suppresses inflammasome-dependent innate immunity. *Nat Commun* **10**, 3493, doi:10.1038/s41467-019-11169-x (2019).
19 Alibayov, B. *et al.* Oxidative Reactions Catalyzed by Hydrogen Peroxide Produced by Streptococcus pneumoniae and Other Streptococci Cause the Release and Degradation of Heme from Hemoglobin. *Infect Immun* **90**, e0047122, doi:10.1128/iai.00471-22 (2022).
20 Surabhi, S. *et al.* Hydrogen Peroxide Is Crucial for NLRP3 Inflammasome-Mediated IL-1beta Production and Cell Death in Pneumococcal Infections of Bronchial Epithelial Cells. *J Innate Immun* **14**, 192-206, doi:10.1159/000517855 (2022).
21 Basavanna, S. *et al.* The effects of methionine acquisition and synthesis on Streptococcus pneumoniae growth and virulence. *PLoS One* **8**, e49638, doi:10.1371/journal.pone.0049638 (2013).
22 Gomez-Mejia, A. *et al.* Pneumococcal Metabolic Adaptation and Colonization Are Regulated by the Two-Component Regulatory System 08. *mSphere* **3**, doi:10.1128/mSphere.00165-18 (2018).
23 van Opijnen, T. & Camilli, A. A fine scale phenotype-genotype virulence map of a bacterial pathogen. *Genome Res* **22**, 2541-2551, doi:10.1101/gr.137430.112 (2012).
24 Crowley, P. J., Gutierrez, J. A., Hillman, J. D. & Bleiweis, A. S. Genetic and physiologic analysis of a formyl-tetrahydrofolate synthetase mutant of Streptococcus mutans. *J Bacteriol* **179**, 1563-1572, doi:10.1128/jb.179.5.1563-1572.1997 (1997).
25 Sah, S., Aluri, S., Rex, K. & Varshney, U. One-carbon metabolic pathway rewiring in Escherichia coli reveals an evolutionary advantage of 10-formyltetrahydrofolate synthetase (Fhs) in survival under hypoxia. *J Bacteriol* **197**, 717-726, doi:10.1128/JB.02365-14 (2015).
26 Aluri, S., Rex, K. & Varshney, U. Simultaneous presence of fhs and purT genes is disadvantageous for the fitness of Escherichia coli growth. *FEMS Microbiol Lett* **362**, doi:10.1093/femsle/fnv101 (2015).
27 Zhanel, G. G. *et al.* Molecular characterisation of Canadian paediatric multidrug-resistant Streptococcus pneumoniae from 1998-2004. *Int J Antimicrob Agents* **28**, 465-471, doi:10.1016/j.ijantimicag.2006.08.005 (2006).
28 Adrian, P. V. & Klugman, K. P. Mutations in the dihydrofolate reductase gene of trimethoprim-resistant isolates of Streptococcus pneumoniae. *Antimicrob Agents Chemother* **41**, 2406-2413, doi:10.1128/AAC.41.11.2406 (1997).
29 Galan, J. E. Salmonella Typhimurium and inflammation: a pathogen-centric affair. *Nat Rev Microbiol* **19**, 716-725, doi:10.1038/s41579-021-00561-4 (2021).
30 Li, G. *et al.* Morin inhibits Listeria monocytogenes virulence in vivo and in vitro by targeting listeriolysin O and inflammation. *BMC Microbiol* **20**, 112, doi:10.1186/s12866-020-01807-6 (2020).
31 Travaglini, K. J. *et al.* A molecular cell atlas of the human lung from single-cell RNA sequencing. *Nature* **587**, 619-625, doi:10.1038/s41586-020-2922-4 (2020).
32 Iliev, A. I. *et al.* Rapid microtubule bundling and stabilization by the Streptococcus pneumoniae neurotoxin pneumolysin in a cholesterol-dependent, non-lytic and Src-kinase dependent manner inhibits intracellular trafficking. *Mol Microbiol* **71**, 461-477, doi:10.1111/j.1365-2958.2008.06538.x (2009).
33 Liu, J. *et al.* Wnt/beta-catenin signalling: function, biological mechanisms, and therapeutic opportunities. *Signal Transduct Target Ther* **7**, 3, doi:10.1038/s41392-021-00762-6 (2022).
34 Herta, T. *et al.* DNA-release by Streptococcus pneumoniae autolysin LytA induced Krueppel-like factor 4 expression in macrophages. *Sci Rep* **8**, 5723, doi:10.1038/s41598-018-24152-1 (2018).
35 Barutcu, A. R. *et al.* SMARCA4 regulates gene expression and higher-order chromatin structure in proliferating mammary epithelial cells. *Genome Res* **26**, 1188-1201, doi:10.1101/gr.201624.115 (2016).

862 36 Wilson, R. *et al.* Protection against Streptococcus pneumoniae lung infection after nasopharyngeal
863 colonization requires both humoral and cellular immune responses. *Mucosal Immunol* **8**, 627-639,
864 doi:10.1038/mi.2014.95 (2015).
865 37 Spellerberg, B. *et al.* Pyruvate oxidase, as a determinant of virulence in Streptococcus pneumoniae.
866 *Mol Microbiol* **19**, 803-813, doi:10.1046/j.1365-2958.1996.425954.x (1996).
867 38 Syk, A. *et al.* Emergence of hypervirulent mutants resistant to early clearance during systemic
868 serotype 1 pneumococcal infection in mice and humans. *J Infect Dis* **210**, 4-13,
869 doi:10.1093/infdis/jiu038 (2014).
870 39 Pericone, C. D., Overweg, K., Hermans, P. W. & Weiser, J. N. Inhibitory and bactericidal effects of
871 hydrogen peroxide production by Streptococcus pneumoniae on other inhabitants of the upper
872 respiratory tract. *Infect Immun* **68**, 3990-3997, doi:10.1128/IAI.68.7.3990-3997.2000 (2000).
873 40 Loose, M. *et al.* Pneumococcal hydrogen peroxide-induced stress signaling regulates inflammatory
874 genes. *J Infect Dis* **211**, 306-316, doi:10.1093/infdis/jiu428 (2015).
875 41 Gonzalez-Juarbe, N. *et al.* Bacterial Pore-Forming Toxins Promote the Activation of Caspases in
876 Parallel to Necroptosis to Enhance Alarmin Release and Inflammation During Pneumonia. *Sci Rep* **8**,
877 5846, doi:10.1038/s41598-018-24210-8 (2018).
878 42 Browall, S. *et al.* Intraclonal variations among Streptococcus pneumoniae isolates influence the
879 likelihood of invasive disease in children. *J Infect Dis* **209**, 377-388, doi:10.1093/infdis/jit481 (2014).
880 43 S., A. FastQC: a quality control tool for high throughput sequence data. (2010).
881 44 Ewels, P., Magnusson, M., Lundin, S. & Kaller, M. MultiQC: summarize analysis results for multiple
882 tools and samples in a single report. *Bioinformatics* **32**, 3047-3048,
883 doi:10.1093/bioinformatics/btw354 (2016).
884 45 Bolger, A. M., Lohse, M. & Usadel, B. Trimmomatic: a flexible trimmer for Illumina sequence data.
885 *Bioinformatics* **30**, 2114-2120, doi:10.1093/bioinformatics/btu170 (2014).
886 46 Langmead, B. & Salzberg, S. L. Fast gapped-read alignment with Bowtie 2. *Nat Methods* **9**, 357-359,
887 doi:10.1038/nmeth.1923 (2012).
888 47 Li, H. *et al.* The Sequence Alignment/Map format and SAMtools. *Bioinformatics* **25**, 2078-2079,
889 doi:10.1093/bioinformatics/btp352 (2009).
890 48 Nicol, J. W., Helt, G. A., Blanchard, S. G., Jr., Raja, A. & Loraine, A. E. The Integrated Genome Browser:
891 free software for distribution and exploration of genome-scale datasets. *Bioinformatics* **25**, 2730-
892 2731, doi:10.1093/bioinformatics/btp472 (2009).
893 49 Liao, Y., Smyth, G. K. & Shi, W. featureCounts: an efficient general purpose program for assigning
894 sequence reads to genomic features. *Bioinformatics* **30**, 923-930, doi:10.1093/bioinformatics/btt656
895 (2014).
896 50 Love, M. I., Huber, W. & Anders, S. Moderated estimation of fold change and dispersion for RNA-seq
897 data with DESeq2. *Genome Biol* **15**, 550, doi:10.1186/s13059-014-0550-8 (2014).
898 51 Yu, G., Wang, L. G., Han, Y. & He, Q. Y. clusterProfiler: an R package for comparing biological themes
899 among gene clusters. *OMICS* **16**, 284-287, doi:10.1089/omi.2011.0118 (2012).
900 52 Rheinwald, J. G. & Green, H. Serial cultivation of strains of human epidermal keratinocytes: the
901 formation of keratinizing colonies from single cells. *Cell* **6**, 331-343, doi:10.1016/s0092-
902 8674(75)80001-8 (1975).
903 53 Carpenter, A. E. *et al.* CellProfiler: image analysis software for identifying and quantifying cell
904 phenotypes. *Genome Biol* **7**, R100, doi:10.1186/gb-2006-7-10-r100 (2006).
905 54 Kirkham, L. A. *et al.* Construction and immunological characterization of a novel nontoxic protective
906 pneumolysin mutant for use in future pneumococcal vaccines. *Infect Immun* **74**, 586-593,
907 doi:10.1128/IAI.74.1.586-593.2006 (2006).

908

Table 1

Pathway	GeneRatio	P-adjust	qvalue
Δ*fhs* vs. WT			
Fatty acid metabolism/biosynthesis	10/57	1.08E-09	6.49E-10
Biosynthesis of secondary metabolites	26/57	2.09E-04	1.26E-04
Purine metabolism	10/57	1.34E-03	8.06E-04
Quorum sensing	11/57	3.20E-03	1.92E-03
Pantothenate and CoA biosynthesis	5/57	3.59E-03	2.16E-03
beta-Lactam resistance	5/57	7.59E-03	4.57E-03
Propanoate metabolism	4/57	1.51E-02	9.09E-03
2-Oxocarboxylic acid metabolism	4/57	1.51E-02	9.09E-03
Metabolic pathways	40/57	1.94E-02	1.16E-02
Amino sugar and nucleotide sugar metabolism	7/57	4.22E-02	2.54E-02
Pyruvate metabolism	5/57	4.31E-02	2.59E-02
Δ*proABC* vs. WT			
Fatty acid metabolism/biosynthesis	10/71	1.17E-08	8.94E-09
Galactose metabolism	12/71	1.25E-04	2.47E-08
Phosphotransferase system (PTS)	13/71	2.54E-03	1.93E-03
Amino sugar and nucleotide sugar metabolism	9/71	2.89E-02	2.20E-02

Figure 1

A

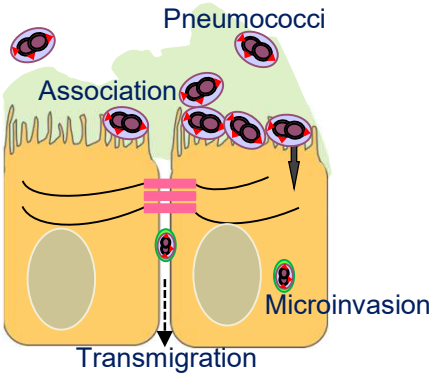

B

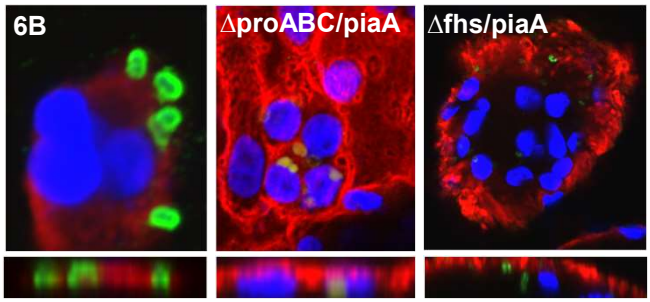

C

	Day 6 post-challenge	
	Association (%)	**Micro-invasion (%)**
6B	87.8 (n11, 43spn)	12.2 (n11, 6spn)
ΔproABC/piaA	59.3 (n11, 16spn)	40.7 (n11, 11spn)
Δfhs/piaA	48.7 (n5, 57spn)	51.3 (n5, 60spn)

D

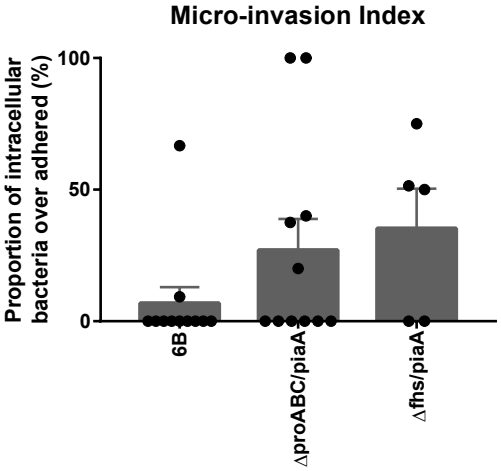

Figure 2

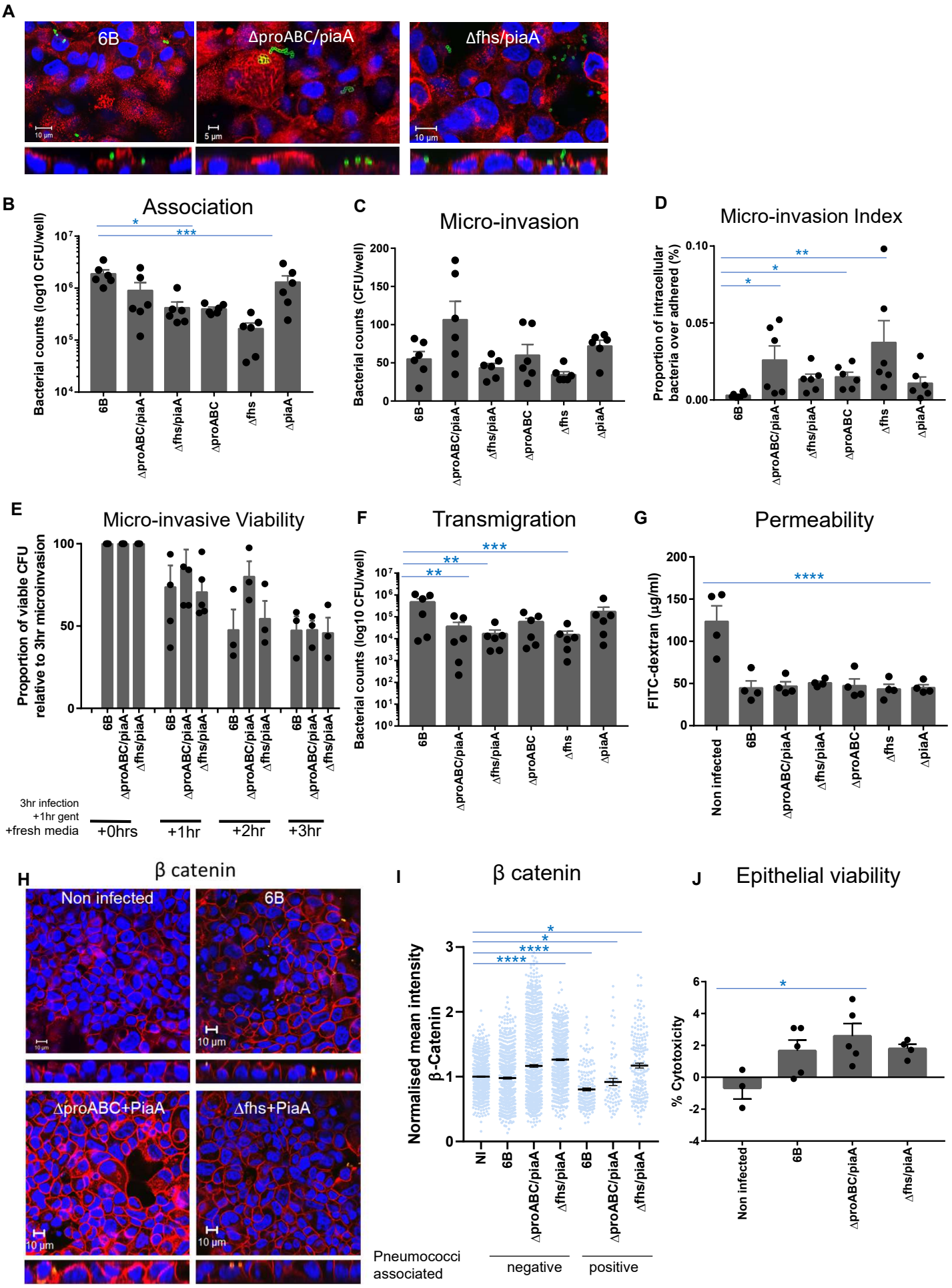
A
6B
ΔproABC/piaA
Δfhs/piaA
10 µm
5 µm
B
Association
Bacterial counts (log10 CFU/well)
6B
ΔproABC/piaA
Δfhs/piaA
ΔproABC
Δfhs
ΔpiaA
C
Micro-invasion
Bacterial counts (CFU/well)
D
Micro-invasion Index
Proportion of intracellular bacteria over adhered (%)
E
Micro-invasive Viability
Proportion of viable CFU relative to 3hr microinvasion
3hr infection
+1hr gent
+fresh media
+0hrs
+1hr
+2hr
+3hr
F
Transmigration
Bacterial counts (log10 CFU/well)
G
Permeability
FITC-dextran (µg/ml)
Non infected
H
β catenin
Non infected
6B
ΔproABC+PiaA
Δfhs+PiaA
I
β catenin
Normalised mean intensity β-Catenin
NI
Pneumococci associated
negative
positive
J
Epithelial viability
% Cytotoxicity

Figure 3

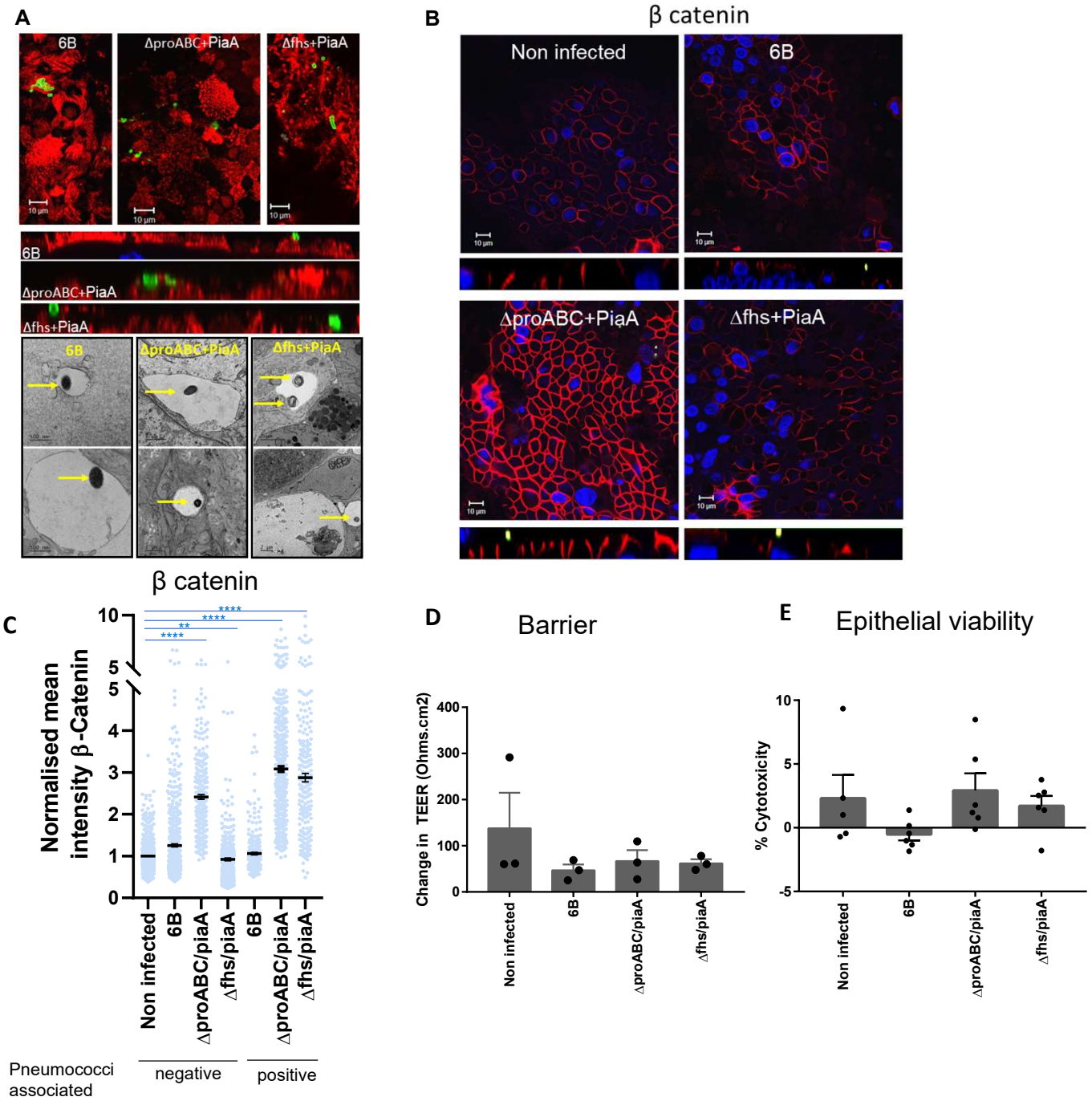
A
6B
ΔproABC+PiaA
Δfhs+PiaA
10 µm
B
β catenin
Non infected
6B
ΔproABC+PiaA
Δfhs+PiaA
C
β catenin
Normalised mean intensity β-Catenin
Non infected
6B
ΔproABC/piaA
Δfhs/piaA
Pneumococci associated
negative
positive
D
Barrier
Change in TEER (Ohms.cm2)
E
Epithelial viability
% Cytotoxicity

Figure 4

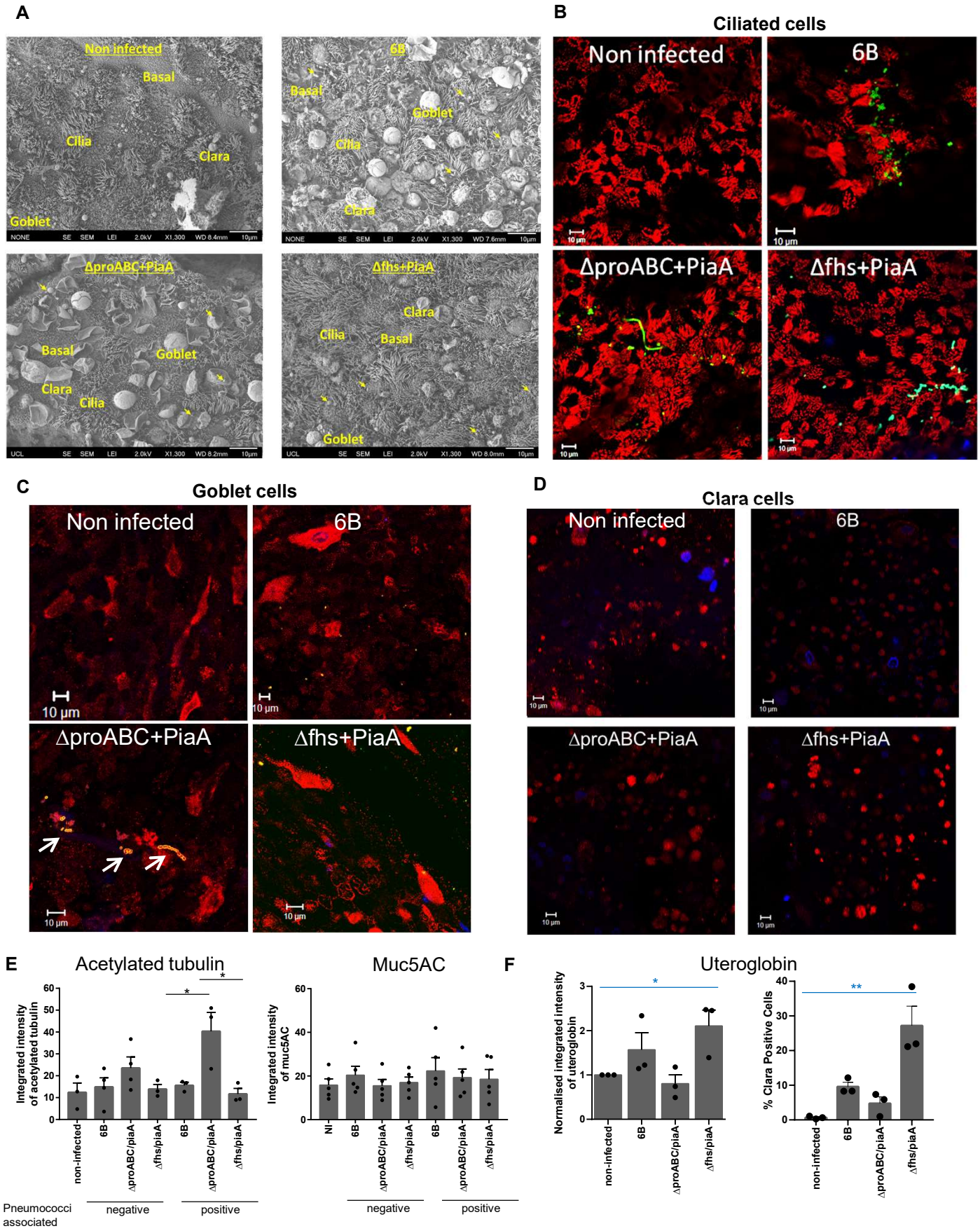
A
Non infected
Basal
Cilia
Clara
Goblet
6B
ΔproABC+PiaA
Δfhs+PiaA
B
Ciliated cells
Non infected
6B
ΔproABC+PiaA
Δfhs+PiaA
C
Goblet cells
Non infected
6B
ΔproABC+PiaA
Δfhs+PiaA
10 µm
D
Clara cells
Non infected
6B
ΔproABC+PiaA
Δfhs+PiaA
E
Acetylated tubulin
Integrated intensity of acetylated tubulin
non-infected
6B
ΔproABC/piaA
Δfhs/piaA
Pneumococci associated
negative
positive
Muc5AC
Integrated intensity of muc5AC
NI
F
Uteroglobin
Normalised integrated intensity of uteroglobin
% Clara Positive Cells

Figure 5

A

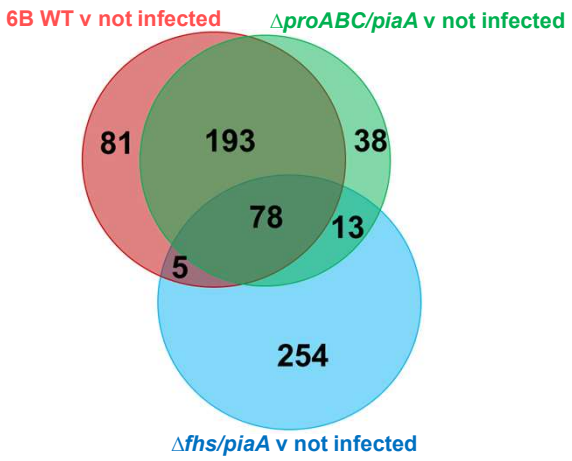

B

log2foldchange	6B	ΔproABC/piaA	Δfhs/piaA
Upregulated genes			
AC256236.1	32.9	25.5	0.0
AC022149.1	30.2	27.6	0.0
Z84488.2	29.1	21.6	0.0
MUC21	25.8	29.0	0.0
VASN	20.9	0.0	0.0
BRD2	18.4	24.7	0.0
AC012254.2	18.2	13.8	0.0
CTAGE4	18.1	0.0	0.0
MICE	17.1	20.3	0.0
AC107075.1	10.1	0.0	0.0
CSNK2B	0.0	20.2	0.0
MTRNR2L6	0.0	19.4	15.8
LSM2	0.0	17.1	0.0
ALOX5	0.0	0.0	6.9
AC006064.6	0.0	0.0	3.4
TAP2	0.0	0.0	3.2
CYP1A1	0.0	0.0	1.7
FOSB	0.0	0.0	1.4
IL1B	0.0	0.0	1.3
CXCL8	0.0	0.0	1.1
CXCL2	0.0	0.0	1.1
CYP1B1	0.0	0.0	1.0

C

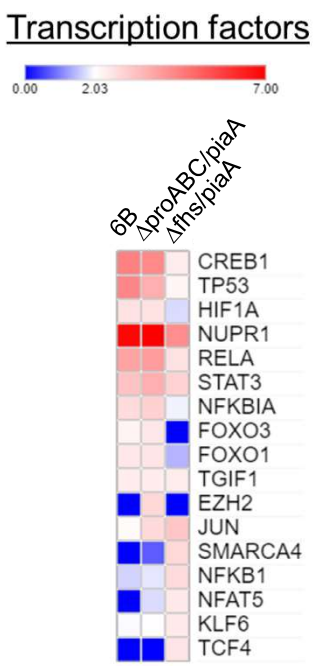

D

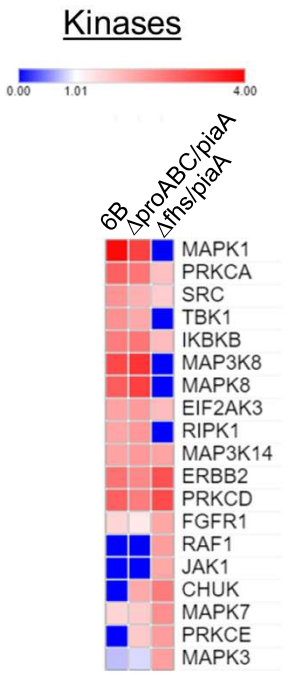

E

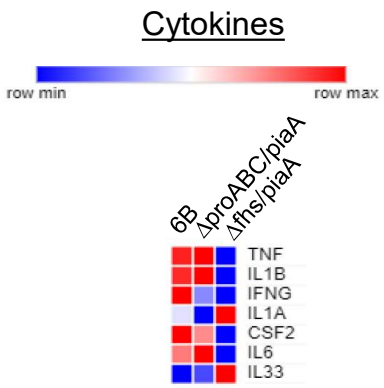

F

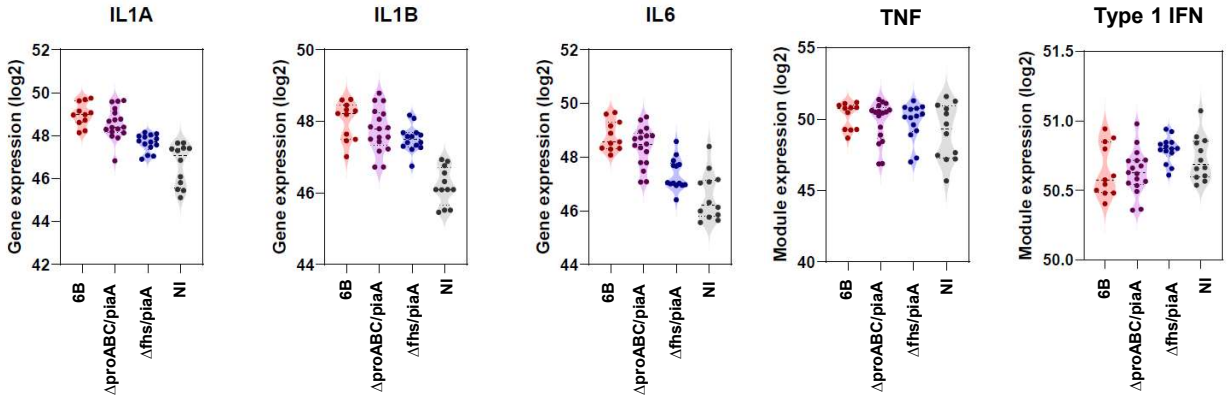

Figure 6

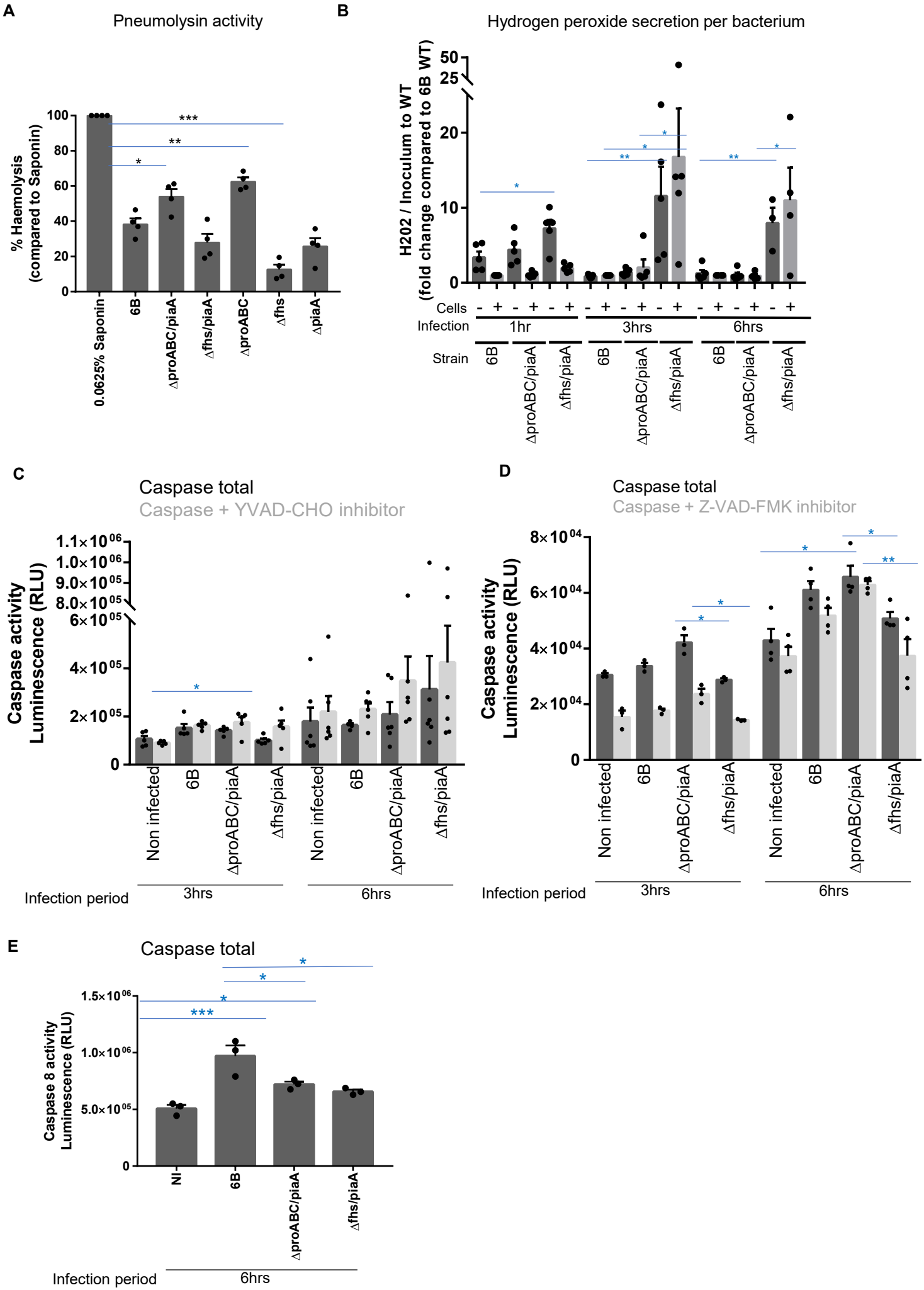
A
Pneumolysin activity
% Haemolysis (compared to Saponin)
100
80
60
40
20
0
***
**
*
0.0625% Saponin
6B
ΔproABC/piaA
Δfhs/piaA
ΔproABC
Δfhs
ΔpiaA
B
Hydrogen peroxide secretion per bacterium
H202 / Inoculum to WT (fold change compared to 6B WT)
50
25
20
10
0
Cells
Infection
1hr
3hrs
6hrs
Strain
6B
ΔproABC/piaA
Δfhs/piaA
C
Caspase total
Caspase + YVAD-CHO inhibitor
Caspase activity Luminescence (RLU)
1.1×10^06
1.0×10^06
9.0×10^05
8.0×10^05
6×10^05
4×10^05
2×10^05
0
Non infected
6B
ΔproABC/piaA
Δfhs/piaA
Infection period
3hrs
6hrs
D
Caspase total
Caspase + Z-VAD-FMK inhibitor
Caspase activity Luminescence (RLU)
8×10^04
6×10^04
4×10^04
2×10^04
0
Non infected
6B
ΔproABC/piaA
Δfhs/piaA
Infection period
3hrs
6hrs
E
Caspase total
Caspase 8 activity Luminescence (RLU)
1.5×10^06
1.0×10^06
5.0×10^05
0
NI
6B
ΔproABC/piaA
Δfhs/piaA
Infection period
6hrs
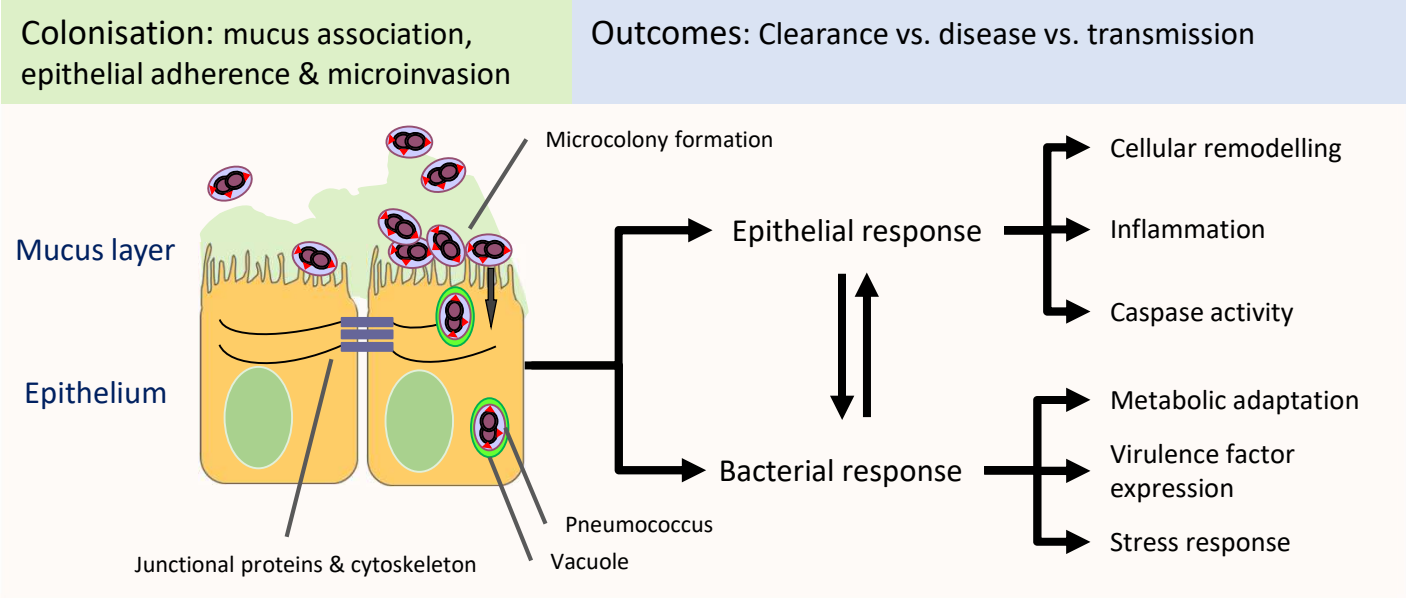
Graphical abstract